Variable Velocity Liquid Flow EPR Applied to Submillisecond Protein Folding

Vladimir M. Grigoryants, Andrei V. Veselov, and Charles P. Scholes
Department of Chemistry, University at Albany, State University of New York, Albany, New York 12222, USA

ABSTRACT　We have developed a variable velocity, rapid-mix, continuous-flow method for observing and delineating kinetics by dielectric resonator-based electron paramagnetic resonance (EPR). The technology opens a new facet for kinetic study of radicals in liquid at submillisecond time resolution. The EPR system (after Sienkiewicz, A., K. Qu, and C. P. Scholes. 1994. *Rev. Sci. Instrum.* 65:68–74) accommodated a miniature quartz capillary mixer with an ≈ 0.5 μL delivery volume to the midpoint of the EPR-active zone. The flow velocity was varied in a preprogrammed manner, giving a minimum delivery time of ≈ 150 μs. The mixing was efficient, and we constructed kinetics in the 0.15–2.1-ms time range by plotting the continuous wave EPR signal taken during flow versus the reciprocal of flow velocity. We followed the refolding kinetics of iso-1-cytochrome *c* spin-labeled at Cysteine 102. At 20°C, upon dilution of guanidinium hydrochloride denaturant, a fast phase of refolding was resolved with an exponential time constant of 0.12 ms, which was consistent with the "burst" phase observed by optically detected flow techniques. At 7°C the kinetic refolding time of this phase increased to 0.5 ms.

INTRODUCTION

Electron paramagnetic resonance (EPR) has not commonly been used for flow and stopped-flow kinetic measurements due to lack of paramagnetic sensitivity from standard metallized EPR cavities and their oversensitivity to vibration and pressure-induced artifacts. As conceived for stopped-flow EPR (Sienkiewicz et al., 1994), our original dielectric resonator (DR) was a combination of a small, high-sensitivity resonator and a microwave-coupling scheme that together were insensitive to stopped-flow induced noisy transients and that provided finesse in tuning and freedom from microphonics. Its initial application was to the protein folding problem (Qu et al., 1997). With yeast iso-1-cytochrome *c* labeled at its naturally occurring Cysteine 102 (C102-SL), we followed the change in the spin-label EPR lineshape that reported nanosecond tumbling motions of the probe while these motions themselves were altered by the kinetics of protein folding. This novel EPR approach was limited by the finite stopping time and dead time between mixing and observation. There was a dead volume in the 5–10 μL range and a 5–10 ms dead time. We were aware that there was a faster component of protein folding that was occurring during the dead time (Table 3 of Qu et al., 1997).

For commonly used UV-Vis and fluorescence stopped-flow methods, rapid kinetic mixing techniques have also generally been limited by the several-millisecond dead time between mixing and detection and by the finite braking time for stopping flow. Faster events in the submillisecond regime have often remained unresolved. Recently, continuous-flow rapid-mix devices monitored with optical and flu-orescence methods have been developed and used for detection of fast biological reactions (Takahashi et al., 1995, 1997; Chan et al., 1997; Shastry et al., 1998; Shastry and Roder, 1998). The flow apparatus of Shastry et al. (1998) was based on a capillary mixer, subsequent to which submillisecond kinetic behavior was followed by scanning the fluorescence with a UV-sensitive charge-coupled device camera along the direction of flow. Tryptophan fluorescence quenching in cytochrome *c*, as brought on by decrease in the distance between the heme iron and the sole tryptophan of cytochrome *c*, was used as an indicator of rapid protein folding (Shastry et al., 1998). Other ultrarapid flow devices, based on UV-Vis or resonance raman spectroscopies, reported heme-dependent optical changes (Takahashi et al., 1995, 1997; Chan et al., 1997; Yeh and Rousseau, 1998, 1999).

We have been motivated to apply flow and stopped-flow kinetics to EPR-detectable, ambient-temperature radicals. The purpose is to open a new area for detecting species that UV-Vis and fluorescence techniques do not observe and for detecting aspects of general processes, such as protein folding, at previously untested locations. In particular, the folding of spin-labeled protein enables one to monitor the en-folding process localized near the labeling site, and with the advent of cysteine-directed mutations, enables one to place monitoring sites at numerous locations not previously probed (Mchaourab et al., 1996). A critical technical development for ultrafast detection is that the DR can be tightly integrated to the mixer structure to obtain time resolution comparable with that of the recent rapid-flow UV-Vis and fluorescence studies. In the case of the above fluorescence-detection scheme (Shastry et al., 1998), kinetic behavior was detected as a distribution of fluorescence intensity in the photodiode array of a charge-coupled device detector. In our method, the position of the DR remains fixed, because scanning it along a direction of flow would be technically impossible. Rather, keeping the distance from mixing to

detector constant, we decrease the age of the kinetically reacting sample by increasing the flow velocity. Thus, a plot of signal size versus inverse velocity provides a profile of the time dependence of the reaction, and we have used a model reaction to calibrate the mixing system and sample age. This method, whose major present motivation is to study fast protein folding, opens a new facet for EPR study of reactions involving liquid radicals at submillisecond time resolution.

INSTRUMENT DESIGN AND CONSTRUCTION

The mixer

The mixer-capillary system shown in Fig. 1 was constructed from calibrated quartz capillary tubing produced by Vitro-Com Inc. (Mountain Lakes, NJ). It was fused with a micro oxygen/hydrogen torch (WaterWelder, Henes Mfg. Co., Phoenix, AZ). Its major components were: two concentric inlet tubes [one having 0.30 mm inside diameter (I.D.) and 0.40 mm outside diameter (O.D.) and the other having 0.60 mm I.D. and 0.84 mm O.D.], a platinum ball mixing element of 0.57-mm diameter, and an outlet tube (0.40 mm I.D., 0.55 mm O.D.). The platinum ball mixer was fused from 0.076-mm platinum wire (Aldrich Chem. Co., Milwaukee, WI) and was suspended within the 0.60-mm I.D. inlet tube. The end of the inner 0.30-mm I.D. delivery tube was nested into a 0.1-mm high frit of 0.076-mm diameter platinum wire just above the platinum ball, and the tip of this 0.30-mm I.D. tube was cut back with two fine fire-polished U-shaped cuts whose purpose was to bifurcate fluid flow in a direction perpendicular to the tube axis. The platinum frit and the bifurcation of the flow eliminated vibration of the internal capillary when the fluid velocity
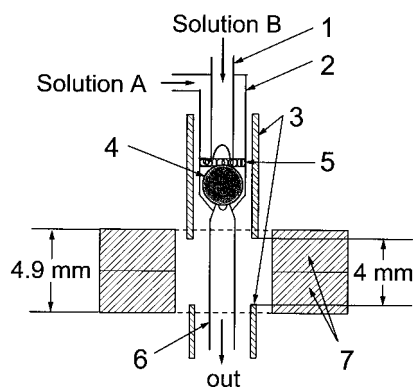

FIGURE 1 Schematic of the micro ball mixer integrated to a 9.5-GHz double dielectric resonator. The system has a delivery (dead) volume between the top of the frit and the center of the EPR observation zone of 0.5 μL. Parts are as follows: *1*, 0.3-mm I.D. inlet capillary; *2*, 0.6-mm I.D. inlet capillary; *3*, 0.9-mm I.D. silver shield tubes; *4*, 0.57-mm Pt sphere; *5*, 0.1-mm frit made from 0.076-mm Pt wire; *6*, 0.4-mm I.D. outlet capillary; *7*, two ceramic toroids of the DR. The height of the double DR structure is 4.9 mm, and the height of the EPR-active zone is 4 mm.

was high. In a configuration similar in principle to that of Shastry et al. (1998) and Regenfuss et al. (1985), fluids from the two inlet tubes flowed past the ball at velocities that gave rise to turbulent mixing in the narrow 0.015-mm annular slit between the ball and the 0.60-mm I.D. tube. The ball itself was placed on top of the 0.40-mm I.D. outlet tube, which had been lightly chipped then fire-polished in such a way as to allow fluid flow past its ball—tube interface and into the 0.40-mm outlet tube. In addition, the ball was centered within the 0.60-mm I.D. inlet tube by several protuberances fused into the wall of that inlet tube. Beyond the point where the ball was seated on the 0.40-mm I.D. outlet tube, there was approximately a 1-mm distance for fluid transport between the ball and the EPR-active zone. The volume of fluid that we directly measured between the beginning of the EPR-active zone of the DR and the top of the frit was 0.25 μL. The volume of the sample tube within the EPR-active zone was 0.50 μL so that the volume from the top of the frit to the center of the EPR-active zone was 0.50 μL.

Integrating the mixer to the dielectric resonator

The 0.40-mm I.D. outlet tube was shielded by a silver 0.90-mm I.D. shield. This shield prevented microwaves from penetrating into the region of mixing and limited the EPR active zone to a 4-mm length within the center of the DR. The basic components of the DR were two back-to-back dielectric ceramic toroids (each 6 mm O.D., 2.45 mm high, 2 mm center hole, $\epsilon = 30$, produced by Murata-Erie, State College, PA) to which microwave-critical coupling was achieved with an adjustable short and coupling loop as previously described in Sienkiewicz et al. (1994). The loaded Q (quality factor) of the device was ~1000. A small set of 100 KHz modulation coils was machined into and wound within the delrin body that enclosed the dielectric resonator. Coolant circulated by a Neslab (Newington, NH) Model RTE-9B Refrigerated Circulating Bath was flowed directly through metal tubes attached to the brass lids of the dielectric resonator outer body and was also flowed through tubes enclosing the sample storage syringes and liquid delivery tubes. Temperature was monitored by a thermocouple mounted on the dielectric resonator.

The liquid drive system

The Model 715 Syringe Ram Controller from Update Instrument, Inc. (Madison, WI), provided synchronizing start pulses for the digitizer card of the PC and provided programmable flow rates and flow times. The controller was modified for a wider range of driver velocities starting from 0.18 cm/s. In our experiments, we used a syringe ram velocity up to 5 cm/s (3.3 μL/ms). For experiments at high velocity, syringe barrels with 6 mm wall thickness and 6.45

mm I.D. were procured from Wilmad Glass Co. (Buena, NJ).

The data acquisition and EPR system

The EPR system was a Bruker ER-200 D-SRC X-band spectrometer which was interfaced to a Compaq 386 PC equipped with IBM analog-to-digital converter and Scientific Software Services Systems (Bloomington, IL) EW 2.41A software for collecting both CW and transient data. For measuring the intensity of the EPR signal during flow, the protocol was to record the EPR time profile during flow (see inset to Fig. 2 A) and to average this EPR signal for a
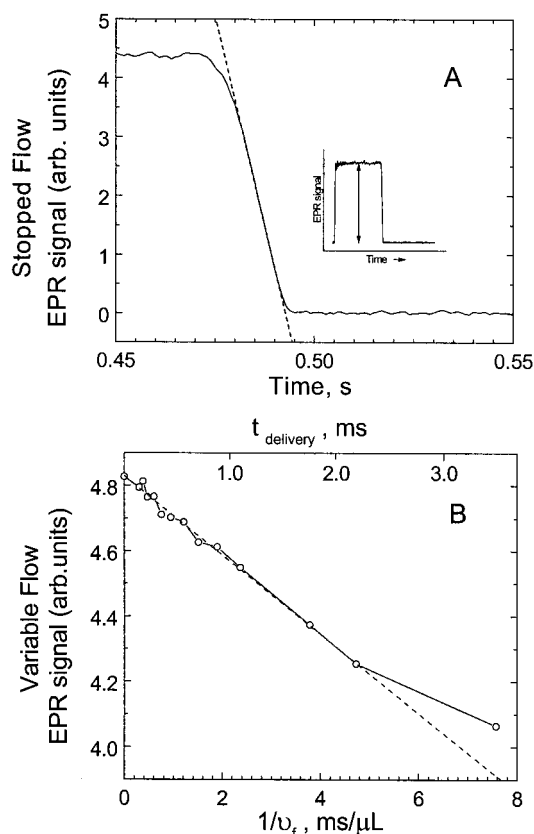

FIGURE 2   This figure presents data useful for flow time calibration. (A) Presents the linear stopped-flow time profile for the decaying EPR signal from 2 mM TEMPO mixed with 30 mM Na-dithionite in 0.1 M KPO$_4$ buffer, pH = 7.2, 20°C, with ram stopping from a 0.26-μL/ms flow velocity. The inset shows a typical EPR signal time profile and amplitude under continuous flow conditions, where the vertical arrow is the EPR signal amplitude during flow. (B) Presents the velocity flow/time calibration curve for our micro ball mixer. We show the dependence of the intensity of the continuously flowing EPR signal upon the reciprocal of the flow velocity for the mixing of the solution of Fig. 2 A, and we show the time scale that we calibrated from the linear decay of the dithionite-TEMPO reaction for delivery of solutions from mixing to the center of the EPR-active zone. Evidence for inefficient mixing was observed at the slowest flow rate (i.e., flow velocity <0. 20 μL/ms or reciprocal velocity >5 ms/μL).

time of 0.1 to 0.3 s (depending on flow velocity) over the data points where the signal had reached a plateau. For determination of the fractional signal intensity, I/I_o, I_o was half the maximal EPR signal measured under stationary conditions before mixing.

OPERATION AND PERFORMANCE

Testing and calibrating

The timing calibration of the instrument was performed by application of a chemical reaction which was empirically and repeatedly found by us to exhibit linear decay, apparently of zeroth order. This reaction was the reductive destruction of the nitroxide TEMPO (2,2,6,6-tetramethyl-4-piperidinol, Sigma) by sodium dithionite (sodium hydrosulfite, Sigma) in 100 mM Na Phosphate buffer, pH 7.2. The concentration of dithionite was adjusted to obtain a linear decay of the signal where the time for complete decay was in the 10–35-ms range. We measured this decay by direct stopped-flow using the present mixer set-up at a number of ram speeds. We started our fitting about 10 ms after the ram stopped to assure that the finite flow-braking time did not interfere with the measurement of the decay. In Fig. 2 A, we show the linear decay of the TEMPO signal resulting from its destruction by dithionite. The linear decay was determined from the average of stopped-flow experiments at different flow rates. The short linear decay time meant that, during flow with delivery times within the 0.15–2.0-ms range, there was a meaningful and detectable change in the EPR as a function of the flow velocity. For a reaction like the TEMPO-dithionite reaction, whose signal decreases linearly with time, it can be shown that the decay of signal intensity depends linearly on the delivery (dead) time between mixing and the center of the EPR-active zone. From this change in the EPR signal, the age of the sample could be determined. In Fig. 2 B, we plot the EPR signal amplitude obtained during flow versus the inverse of the flow velocity. This plot was also made against a delivery time that was the age of the sample computed from the linearly decaying, previously calibrated, amplitude of the EPR signal. At all but the slowest velocity (as discussed in the next paragraph), the signal amplitude scaled linearly with the inverse of flow velocity. The implications of this linear scaling were: first, that the calibration reaction continued to be linear in time even for short times below 1 ms, and second, that the actual time for turbulent mixing in the narrow annular region near the ball (Regenfuss et al., 1985) was much less than the dead time for the sample to flow from mixer to the EPR-active volume, at all but the slowest velocity. The dead volume obtained from the calibrating chemical reaction (see text above and the Appendix) was about 0.45 μL. This volume was about 0.05 μL less than the 0.50 μL volume that was physically measured from the top of the frit (Fig. 1) to the center of the EPR-active zone. The

liquid volume, which we directly measured from the top of the frit to the middle of the ball, was 0.05–0.06 μL. Therefore, we concluded that the capillary system has an effective mixing area located near the narrow slit between the tube and the ball; this slit occurs approximately at the middle of the ball.

The ball mixer and tubes that we use are several times larger than those used in the design of Shastry et al. (1998) because the volume of reactant needed for EPR is larger than for fluorescence. Nevertheless, the larger sizes provide good mixing except at our lowest velocities and longest delivery times (>2 ms), where there was evidence for inefficient mixing because the signal during flow deviated in a positive direction from linear decay as shown in Fig. 2 *B*. The positive deviation of signal at slowest velocity implies that the chemical reaction for these slowest flows had not proceeded as far as expected because the reactants were slow to mix. In other words, at the slowest velocity, the time for efficient mixing was evidently not much less than the time for the sample to flow from the mixing element to the EPR-active volume. Fortunately, kinetic behavior in the >2-ms time regime can be independently obtained by the stopped-flow method with the velocity before stopping >0.2 μL/ms.

The age of a small flowing volume element of sample within the EPR active volume will depend on its distance from the mixer and upon the flow velocity. In summary: we had determined (above) that efficient mixing had already occurred in the mixing area near the ball, and therefore, the age of a differential sample element within the DR was proportional to the volume of fluid between that sample element and the mixing region and inversely proportional to the flow velocity. To simulate the signal amplitude as a function of flow velocity in the presence of exponential protein-folding kinetics, an equation describing kinetic behavior with one or two exponential decays was convoluted with the expected position- and velocity-dependent age of the sample within the DR. The variation in EPR sensitivity along the axis of the DR also was included in the convolution. [The EPR sensitivity throughout the EPR active zone of our DR device was measured with a point DPPH (2,2-diphenyl-1-picrylhydrazyl, Sigma) source. The sensitivity profile was found to be symmetric about the center of the DR and bound in the form of a parabola.] The kinetic parameters (exponential amplitudes and exponential rate constants) were extracted from a least squares fit of experimental signal amplitude to simulated signal amplitude at different flow velocities. A detailed explanation is given in the Appendix indicating how the simulation of the variable velocity flow EPR signal amplitude and the subsequent fit to experimental data were carried out. As discussed below, the results of such fits are shown in the curves of Fig. 4, *A* and *B*.

The application to the folding of spin-labeled protein

Experiments were carried out on C102-SL, which is wild type yeast iso-1-cytochrome *c* labeled at its naturally occurring Cys102 sulfur with the cysteine-specific spin label methanethiosulfonate spin label (MTSSL, Reanal Fine Chemicals, Budapest, Hungary). For this study, we used commercial yeast cytochrome (*Saccharomyces cerevisiae,* Sigma). The detailed preparation of C102-SL, together with its characterization and EPR spectra, is provided in Qu et al. (1997). To refold, we mixed protein unfolded in GdnHCl (guanidinium hydrochloride ultrapure, Sigma) with dilute pH 5.0 Na acetate buffer to reach a GdnHCl concentration where the protein refolded. Figure 3 compares the room temperature EPR spectra of unfolded and ≈70% refolded C102-SL at the same protein concentration, but respectively, in 0.8 M GdnHCl and 0.4 M GdnHCl. We set the magnetic field at the peak of the central EPR feature and used our variable velocity flow method for the time regime <2 ms and our stopped-flow method for the time regime >2 ms. We observed how the fractional amplitude of the signal decreased with time. As shown in Fig. 4 *A*, at room temperature, there was an ≈37% component of the folding that occurred in a time less than 400 μs with an exponential decay time of 0.12 ± 0.02 ms, and there was another ≈63% component that had an exponential decay time of 6.2 ± 0.8 ms. Direct stopped-flow EPR given in Fig. 5 *A* showed a 7 ± 2-ms component to the refolding, consistent with the 6.2-ms component obtained by the variable velocity flow method. In doing the set of variable velocity flow measurements of rapid folding (Fig. 4 *A*), we used approximately 2 mL of 0.4 mM C102-SL, and, in obtaining the stopped-flow results (Fig. 5 *A*) with 7-ms decay, we also used about 2 mL of 0.4 mM C102-SL. The exponential time of 0.12 ms at 20°C is comparable with the early 50-μs folding process measured by Shastry et al. (1998). [It should be noted that
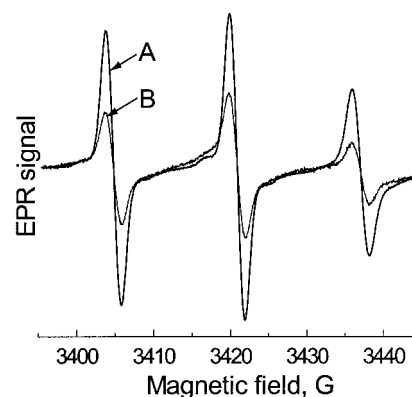

FIGURE 3 Overlay of the absorption derivative (dχ"/d*H*) EPR spectra of 0.4 mM C102-SL (*A*) in 0.8 M GdnHCl, 0.1 M Na Acetate, pH 5.0 and (*B*) in 0.4 M GdnHCl, 0.1 M Na Acetate, pH 5.0. Gain = 6.3 × 10^5; modulation = 1.8 G; time constant = 1 ms; power = 0.4 mWatt.
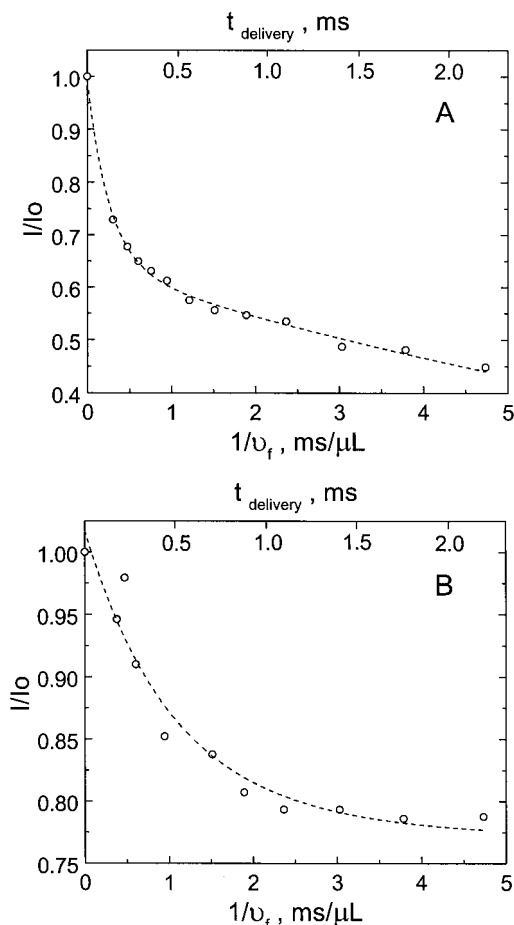
FIGURE 4   (A) The decreasing amplitude of the EPR signal at 20°C represented by the fractional signal intensity I/I_o ($\bigcirc$). 0.4 mM spin-labeled C102-SL in 0.8 M GdnHCl was mixed 1:1 with dilute 0.1 M Na acetate buffer to obtain a 0.4 M GdnHCl concentration in which the protein was ≈70% refolded. The decrease of the central EPR feature from folding protein is shown as a function of the inverse of flow velocity (*lower horizontal axis*) and of the calibrated delivering time (*upper horizontal axis*) between the mixer and the center of the observation EPR zone. The fit (*dashed lines*) indicates the presence of two components of the folding processes, one with a 0.12 ± 0.02-ms exponential decay and the other with a 6.2 ± 0.8-ms exponential decay. The former had an amplitude that was ≈37% of the signal change, and the latter had an amplitude that was ≈63% of the signal change. (B) The decreasing fractional amplitude taken at 7°C, where there was only one component in the 0.1–2-ms range whose decay time was 0.5 ± 0.05 ms; this phase accounted for ≈25% of the overall signal change.

the work of Shastry was carried out on horse cytochrome *c* and with different folding conditions, whereby unfolded protein at pH 2.0 was mixed with buffer to cause folding at pH 4.5.] The 6.2-ms decay is comparable with the longer millisecond phase thought to indicate the reformation of tertiary contacts when refolding occurs in the pH 5 regime (Roder et al., 1988; Elöve et al., 1992, 1994; Colón et al., 1996). At a lower, 7°C, temperature, the submillisecond process was slower and had an exponential relaxation time of 0.5 ± 0.05 ms (Fig. 4 *B*), and the former millisecond
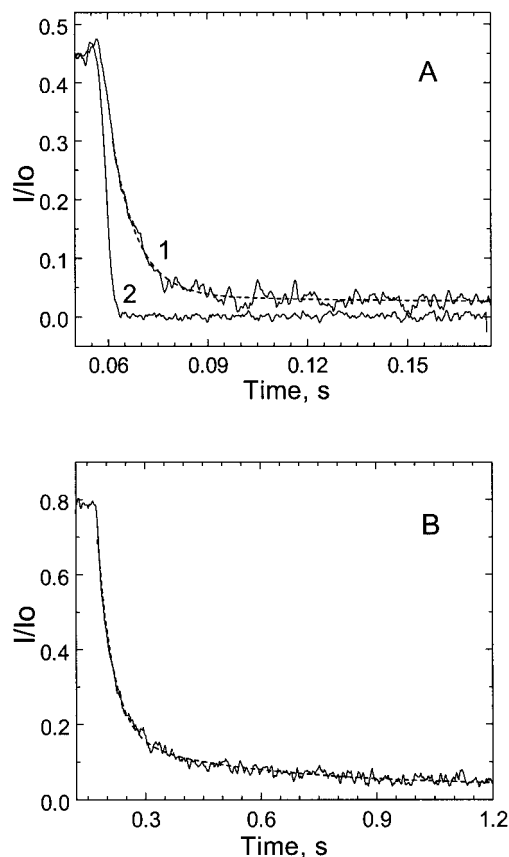

FIGURE 5   (A) The stopped-flow kinetics (*curve 1*) measured at 20°C represented by the fractional signal intensity I/I_o under the same solution mixing conditions as Fig. 4 *A*. In this case, there was a rapid transient showing a time decay of 7 ± 2 ms. Because there is a finite fast braking time for the flow, we also provide the profile of a very fast reaction (*curve 2*) of TEMPO with dithionite (1 mM TEMPO + 1 M dithionite), which represents the apparatus slowing function. (B) The stopped-flow kinetics measured at 7°C under the same solution mixing conditions as Fig. 4 *B*. The phase with 40 ± 2-ms decay time accounted for ≈65% of the overall signal change, a slow phase with 0.38-s decay time accounted for ≈10% of the overall signal change, and the 0.5 ± 0.05-ms phase (Fig. 4 *B*) accounted for ≈25% of the overall signal change.

process had now extended in time to a major phase with a decay time of 40 ± 2 ms and a minor phase with decay time of 0.38 s (Fig. 5 *B*). For resolving the 40-ms process and the 0.38-s processes at 7°C with stopped-flow EPR, about 0.5 mL of reactant was needed, because less signal averaging was required than for resolving the 7-ms process by stopped-flow at 20°C. It is clear from the comparison of kinetics at 7 and 20°C that there is a significant temperature dependence to the rates of both the submillisecond and the millisecond and longer processes. As shown by SDS PAGE gels, there was no damage to the protein by the rapid mix process even at highest velocities. Furthermore, there was no transient tendency of the rapid mixer to reversibly unfold the protein at high flow velocity as shown by a constant signal when two protein solutions at the same identical 0.4-M or 0.8-M GdnHCl concentrations were rapidly mixed.

CONCLUSION

Our DR-based EPR system is now realized and has been tested for doing variable-velocity flow measurements to resolve fast submillisecond kinetic components. In our method, the position of the active zone for detecting a signal remains constant, but the age of the sample is varied by varying the flow rate. This is the flow method needed when the area for detecting the signal cannot be moved. We have shown the significance of our technique to measuring protein folding where the submillisecond component of folding is reported by a probe that is attached and enfolded at a position that is ~15 Å from the heme (Qu et al., 1997). The millisecond and submillisecond refolding times are comparable with those that have been measured by Trp59 fluorescence quenching that is sensitive to change in the heme-Trp59 distance (Shastry et al., 1998) and by UV-Vis and Raman that are sensitive to heme ligation (Takahashi et al., 1997; Yeh and Rousseau, 1998, 1999). Thus, the spin label reports a rapid phase consistent with rapid collapse (Chan et al., 1997) and a longer millisecond phase that is consistent with the reformation of tertiary contacts (Roder et al., 1988; Elöve et al., 1992, 1994; Colón et al., 1996). What remains to be determined is whether probes at other positions than Cys102 throughout the protein will report a similar collapse and similar slower phenomena or whether one or both of these kinetic phases depends on where within the protein the probing occurs. Experiments with MTSSL positioned at different cysteine-mutated sites throughout the protein are underway.

APPENDIX

We first explain the simulation of the EPR amplitude for a flowing, spin-labeled sample within the DR when there are exponentially decaying components to that spin-label signal. We next discuss the method whereby the delivery (dead) volume was determined in the course of calibration.

The EPR signal (I) recorded in variable-velocity flow experiments can be represented as an averaged (i.e., integrated) signal over the whole EPR-active zone (DR window),

$$\langle I(v^{-1})\rangle = \int I(x/v) \cdot f(x)\mathrm{d}x \Big/ \int f(x)\mathrm{d}x, \qquad (A1)$$

where, $I(x/v)$ is the intensity of the EPR signal from a differential volume of sample having coordinate x, and v is the linear velocity of flow. The ratio x/v would be the "aging" time for the liquid sample to reach after mixing the coordinate x at the flow velocity v. For protein-folding behavior, a two-component exponential decay of the form $I(x/v) = \{A_1 \cdot \exp[-(x/v)/\tau_1] + A_2 \cdot \exp[-(x/v)/\tau_2]$ is taken. $f(x)$ is the EPR sensitivity function within the DR window. $f(x)$ had been experimentally measured (see text) and accurately found to be a parabola that was maximal at the center of the DR structure and which went to zero on the boundaries of the DR window as limited by the silver tube shields. The form of Eq. A1 remains the same if the linear velocity (v) in Eq. A1 is replaced with the volume flow rate (v_f) and if the linear dimensions (x) of the sample along the DR is replaced with the volume of sample tube (V) along the DR. It then follows that the integration of

Eq. A1 for an exponential kinetic decay with two components gives

$$\left\langle \frac{I(v_f^{-1})}{I_o}\right\rangle = A_1 \cdot 3 \cdot \left(\frac{\tau_1}{\Delta t}\right)^2 \cdot \exp\left(-\frac{t_d}{\tau_1}\right)$$
$$\cdot \left[\cosh\left(\frac{\Delta t}{\tau_1}\right) - \left(\frac{\tau_1}{\Delta t}\right)\cdot\sinh\left(\frac{\Delta t}{\tau_1}\right)\right]$$
$$+ A_2 \cdot 3 \cdot \left(\frac{\tau_2}{\Delta t}\right)^2 \cdot \exp\left(-\frac{t_d}{\tau_2}\right)$$
$$\cdot \left[\cosh\left(\frac{\Delta t}{\tau_2}\right) - \left(\frac{\tau_2}{\Delta t}\right)\cdot\sinh\left(\frac{\Delta t}{\tau_2}\right)\right], \qquad (A2)$$

where I_o is the initial intensity of the signal, v_f is the liquid sample volume flow rate, A_1 and A_2 are relative contributions of exponential components with τ_1 and τ_2 decay times. $t_d = V_d/v_f$ is the delivery time, and it is the time needed to fill up the delivery volume V_d, which is the dead volume between the mixing area and the middle of the DR window. $\Delta t = V_w/v_f$ is the time needed to fill half the volume of the DR window, where $2V_w (= 0.50\ \mu L)$ is the volume of the DR window. To obtain estimates of the kinetic parameters A_1, A_2, τ_1, and τ_2, we computed for various values of v_f the sum of squares of errors between Eq. A2 and the experimentally determined variable velocity flow EPR signal. A standard nonlinear least squares fitting routine (Origin 3.5, Microcal Software, Inc., Northhampton, MA) was then used to obtain the kinetic parameters A_1, A_2, τ_1, and τ_2.

The delivery (dead) volume V_d and a timing calibration of the variable velocity flow scale were obtained by comparing the linear decay, ΔI, of the signals in the reaction of TEMPO and sodium dithionite (see text) from stopped-flow measurements and from variable-velocity flow experiments. For the stopped-flow measurements,

$$\langle \Delta I(t)\rangle = k\Delta t_{SF}. \qquad (A3)$$

For the variable velocity flow measurements,

$$\langle \Delta I(V_d/v_f)\rangle = k\Delta(V_d/v_f)_{VVF}, \qquad (A4)$$

where k is the decay constant, Δt_{SF} and $\Delta(V_d/v_f)_{VVF}$ are timing intervals for stopped-flow and variable velocity flow measurements, respectively. When $\langle \Delta I(t)\rangle = \langle \Delta I(V_d/v_f)\rangle$, $\Delta t_{SF} = \Delta(V_d/v_f)_{VVF}$. Because we knew v_f from the syringe velocity (in particular, when it was 1 cm/s) and from the cross-sectional areas of the syringes, we could then calculate V_d, which was about 0.45 μL.

REFERENCES

Chan, C.-K., Y. Hu, S. Takahashi, D. L. Rousseau, W. A. Eaton, and J. Hofrichter. 1997. Submillisecond protein folding kinetics studied by ultrarapid mixing. *Proc. Natl. Acad. Sci. USA.* 94:1779–1784.

Colón, W., G. A. Elöve, L. P. Wakem, F. Sherman, and H. Roder. 1996. Side chain packing of the N- and C-terminal helices plays a critical role in the kinetics of cytochrome *c* folding. *Biochemistry.* 35:5538–5549.

Elöve, G. A., A. K. Bhuyan, and H. Roder. 1994. Kinetic mechanism of cytochrome *c* folding: involvement of the heme and its ligands. *Biochemistry.* 33:6925–6935.

Elöve, G. A., A. F. Chaffotte, H. Roder, and M. E. Goldberg. 1992. Early steps in cytochrome *c* folding probed by time-resolved circular dichroism and fluorescence spectroscopy. *Biochemistry.* 31:6876–6883.

Mchaourab, H. S., M. A. Lietzow, K. Hideg, and W. L. Hubbell. 1996. Motion of spin-labeled side chains in T4 Lysozyme. Correlation with protein structure and dynamics. *Biochemistry.* 35:7692–7704.

Qu, K., J. L. Vaughn, A. Sienkiewicz, C. P. Scholes, and J. S. Fetrow. 1997. Kinetics and motional dynamics of spin labeled yeast Iso-1-cytochrome c. 1. Stopped-flow EPR as a probe for protein folding/unfolding of the C-terminal helix spin labeled at Cysteine 102. *Biochemistry.* 36:2884–2897.

Regenfuss, P., R. M. Clegg, M. J. Fulwyler, F. J. Barrentes, and T. M. Jovin. 1985. Mixing liquids in microseconds. *Rev. Sci. Instrum.* 56: 283–290.

Roder, H., G. A. Elöve, and S. W. Englander. 1988. Structural characterization of folding intermediates in cytochrome *c* by H-exchange labeling and proton NMR. *Nature.* 335:700–704.

Shastry, M. C. R., S. D. Luck, and H. Roder. 1998. A continuous-flow capillary mixing method to monitor reactions on the microsecond time scale. *Biophys. J.* 74:2714–2721.

Shastry, M. C. R., and H. Roder. 1998. Evidence for barrier-limited protein folding kinetics on the microsecond time scale. *Nature Struct. Biol.* 5:385–392.

Sienkiewicz, A., A. M. da Costa Ferreira, B. Danner, and C. P. Scholes. 1999. Dielectric resonator-based flow and stopped-flow EPR with rapid field scanning: a methodology for increasing kinetic information. *J. Magn. Reson.* 136:137–142.

Sienkiewicz, A., K. Qu, and C. P. Scholes. 1994. Dielectric resonator-based stopped-flow EPR. *Rev. Sci. Instrum.* 65:68–74.

Takahashi, S., Y.-c. Ching, J. Wang, and D. L. Rousseau. 1995. Microsecond generation of oxygen-bound cytochrome *c* oxidase by rapid solution mixing. *J. Biol. Chem.* 270:8405–8407.

Takahashi, S., S.-R. Yeh, T. K. Das, C.-K. Chan, D. S. Gottfried, and D. L. Rousseau. 1997. Folding of cytochrome *c* initiated by submillisecond mixing. *Nature Struct. Biol.* 4:44–50.

Yeh, S.-R., and D. L. Rousseau. 1998. Folding intermediates in cytochrome *c. Nature. Struct. Biol.* 5:222–228.

Yeh, S.-R., and D. L. Rousseau. 1999. Ligand exchange during unfolding of cytochrome c. *J. Biol. Chem.* 274:17853–17859.